2014

Energy-resolved collision-induced dissociation pathways of model N-linked glycopeptides: implications for capturing glycan connectivity and peptide sequence in a single experiment

Venkata Kolli
University of Nebraska-Lincoln

Eric D. Dodds
University of Nebraska-Lincoln, edodds2@unl.edu

Analyst

PAPER

View Article Online
View Journal | View Issue

Cite this: *Analyst*, 2014, **139**, 2144

Energy-resolved collision-induced dissociation pathways of model N-linked glycopeptides: implications for capturing glycan connectivity and peptide sequence in a single experiment†

Venkata Kolli and Eric D. Dodds*

Tandem mass spectrometry (MS/MS) of glycopeptides stands among the principal analytical approaches for assessing protein glycosylation in a site-specific manner. The aims of such experiments are often to determine the monosaccharide connectivity of the glycan, the amino acid sequence of the peptide, and the site of glycan attachment. This level of detail is often difficult to achieve using any single ion dissociation method; however, precedent does exist for use of collision-induced dissociation (CID) to establish either the connectivity of the oligosaccharide or the sequence of the polypeptide depending upon the applied collision energy. Unfortunately, the relative energy requirements for glycan and peptide cleavage have not been thoroughly characterized with respect to specific physicochemical characteristics of the precursor ions. This report describes case studies on the energy-resolved CID pathways of model tryptic glycopeptides derived from *Erythrina cristagalli* lectin and bovine ribonuclease B. While glycopeptide ions having disparate physical and chemical characteristics shared strikingly similar qualitative responses to increasing vibrational energy deposition, the absolute collision energies at which either glycan or peptide fragmentations were accessed varied substantially among the precursor ions examined. Nevertheless, these data suggest that the energy requirements for peptide and glycan cleavage may be somewhat predictable based on characteristics of the precursor ion. The practical usefulness of these observations was demonstrated through implementation of online collision energy modulation such that both glycan and peptide fragmentation were captured in the same spectrum, providing near-exhaustive glycopeptide characterization in a single experiment. Overall, these results highlight the potential to further extend the capabilities of CID in the context of glycoproteomics.

Received 18th December 2013
Accepted 4th March 2014

DOI: 10.1039/c3an02342g

www.rsc.org/analyst

Introduction

The site-specific analysis of protein glycosylation in complex biological samples stands among the grand challenges facing modern post-genomic science.[1–5] Accordingly, there exists a strong demand for glycoproteomic capabilities to facilitate determination of site-specific glycosylation in biological mixtures. This interest has been motivated in large part by a continually expanding appreciation of protein-modifying oligosaccharides as they pertain to numerous biological processes (*e.g.*, fertilization; immune recognition; host–pathogen interaction; *etc.*) and human disease states (*e.g.*, cancer; congenital disorders of glycosylation; neurodegenerative disorders, *etc.*).[6–17] While protein glycosylation analyses are often carried out with either a "glycocentric" (*i.e.*, compositional and structural analysis of glycans released from glycoproteins) or a "proteocentric" (*i.e.*, identification of deglycosylated glycoproteins with indirect glycosylation site localization) outlook, the loss of molecular detail imposed by glycan release limits the specificity and potential for biological resolution that can be furnished by such analyses.[18] In order to map specific oligosaccharide structures to their corresponding sites of protein attachment, the analytical scheme must preserve the oligosaccharide–polypeptide connectivity until such a time that the chosen approach can characterize the linkage.

One means of addressing this task entails the adaptation of bottom-up methods for mass spectrometry (MS) based proteomics to characterize glycopeptides.[19–21] While advantageous in terms of directness (glycan release is avoided, thus attachment sites need not be merely inferred), this approach is subject to a number of analytical challenges.[22,23] The acquisition and subsequent interpretation of informative tandem mass spectrometry (MS/MS) data for glycopeptide ions stand among the most pressing of these challenges. Significant effort has been

Department of Chemistry, University of Nebraska – Lincoln, Lincoln, NE 68588-0304, USA. E-mail: edodds2@unl.edu; Fax: +1-402-472-9402; Tel: +1-402-472-3592

† Electronic supplementary information (ESI) available: As noted in the text, CID spectra and energy-resolved CID data are provided for the doubly protonated ECL glycopeptide and the triply protonated BRB glycopeptide. See DOI: 10.1039/c3an02342g

made to maximize the information content of glycopeptide ion dissociation spectra, including those obtained through vibrational activation/dissociation methods such as collision-induced dissociation (CID)[24,25] and infrared multiphoton dissociation (IRMPD);[26,27] ion–electron and ion–ion reactions resulting in electron capture dissociation (ECD)[28,29] or electron transfer dissociation (ETD);[30,31] and irradiation with ultraviolet photons in order to achieve ultraviolet photodissociation (UVPD).[32,33] One useful outcome of these investigations has been the observation of a high degree of complementarity between the vibrational activation/dissociation spectra and the electron capture/transfer dissociation spectra of glycopeptide ions. A number of researchers have noted that while CID and IRMPD tend to preferentially cleave the oligosaccharide moiety, ECD and ETD characteristically result in cleavage of only the polypeptide backbone.[34–38] This general behavior has proven very valuable, as application of two complementary methods can enable thorough characterization of glycopeptide composition and structure.[39–43] Unsurprisingly, a number of other glycopeptide ion dissociation pathways have been observed which do not fall within the domain of strictly complementarity vibrational activation/dissociation and electron transfer/capture dissociation.[44–47] This includes numerous examples of vibrational activation/dissociation methods providing information not limited to the carbohydrate group, but extending to the amino acid sequence of the peptide group as well. For example, fragmentation of glycopeptide amino acid chains has been noted in IRMPD,[26,27,48,49] low-energy beam-type CID,[50–54] and high-energy beam-type CID.[55–57] As noted in these studies, the energy required to achieve scission of the peptide backbone is generally much greater than that necessary for cleavage of the glycan group. These energy-resolved fragmentation channels are of significant analytical utility; however, the various dissociation pathways have not been thoroughly studied with respect to specific physical and chemical characteristics of glycopeptide precursor ions. In particular, the present understanding of factors which dictate the energetic requirements for peptide backbone fragmentation is not well developed, despite even relatively recent energy-resolved CID studies of glycopeptides (which did not investigate the fragmentation of the peptide group).[25,58] This type of understanding would be of great practical use, as it could conceivably allow precursor ion characteristics to inform the setting of CID collision energies such that glycan or peptide cleavages are more deliberately accessed. If well characterized, the diverse fragmentation pathways of glycosylated peptide ions can be highly advantageous in increasing the density of structural information yielded by MS/MS. Moreover, as essentially all MS/MS instruments are capable of CID, the ability to extract maximum structural information regarding both the oligosaccharide and the polypeptide using low-energy vibrational activation/dissociation alone is particularly appealing.

The research reported here is focused upon a detailed study of the energy-resolved CID characteristics of tryptic glycopeptides chosen as models for this study due to their disparate characteristics. The first of these was a 17 amino acid glycopeptide carrying a seven monosaccharide paucimannosidic glycan (*i.e.*, containing the trimannosyl core with added fucose and xylose residues). The second was a six amino acid glycopeptide carrying a seven monosaccharide high mannose glycan (*i.e.*, containing the trimannosyl core with added mannose residues). These model glycopeptides, each harboring two basic amino acid side chains, were studied as their doubly protonated and triply protonated precursor ions. This allowed the energy requirements of the various fragmentation pathways to be evaluated both in the presence and absence of readily mobile protons. Although there were considerable quantitative differences in the absolute collision energies at which different dissociation channels were accessed, these experiments revealed a striking concordance with respect to qualitative trends in the energy-resolved CID behaviors of these analytes. In all cases, Y-type fragmentations of the oligosaccharide group comprised the lowest-energy dissociation pathways; however, with increasing vibrational energy deposition these primary fragment ions gave rise to secondary product ions dominated by the Y_1 fragment (peptide plus reducing terminal monosaccharide) and ultimately a collection of tertiary fragments including the Y_0 fragment (complete glycan loss) and an abundance of peptide b and y fragments. Despite the quantitative differences in energy-resolved CID of the precursor ions examined, these data suggest that key dissociation characteristics may be somewhat predictable based on characteristics of the precursor ion. Finally, these observations enabled the design and implementation of a multi-energy CID experiment which permitted different energy-resolved dissociation channels to be captured in a single information-rich CID spectrum which yielded both the glycan connectivity and the amino acid sequence. In summary, the present results suggest means of taking more complete advantage of CID capabilities for glycopeptide structure characterization.

Materials and methods

Chemicals

Bovine ribonuclease B (BRB), ammonium bicarbonate, urea, dithiothreitol, iodoacetamide, proteomics grade trypsin, imidazole, and formic acid were purchased from Sigma-Aldrich (St. Louis, MO, USA). *Erythrina cristagalli* lectin (ECL) was obtained from Vector Labs (Burlingame, CA, USA). HPLC grade acetonitrile was acquired from Fisher Scientific (Fair Lawn, NJ, USA). HPLC grade water was purchased from Burdick & Jackson (Muskegon, MI, USA).

Sample preparation

For each glycoprotein of interest, a 50 μL aliquot of 2 μg μL^{-1} glycoprotein solution in 8 M urea and 50 mM NH_4HCO_3 (pH 7.5) was treated with 10 μL of 450 mM dithiothreitol in 50 mM NH_4HCO_3 (pH 7.5). This mixture was incubated for 1 h at 55 °C for disulfide bond reduction. A 10 μL portion of 500 mM iodoacetamide in 50 mM NH_4HCO_3 (pH 7.5) was then added. This was followed by incubation for 1 h in the dark at ambient temperature for thiol acetamidation. The urea content of the sample was then diluted to < 2 M by addition of 175 μL 50 mM

NH_4HCO_3 (pH 7.5). A 5 μL aliquot of 0.5 μg μL^{-1} of trypsin was next added, and this solution was allowed to incubate for 18 hours at 37 °C. The digest was subsequently vacuum centrifuged using a Speed Vac SC110 (Thermo Savant, Holbrook, NY, USA) to reduce the volume of the solution to approximately 10 μL. The digest was reconstituted to a total volume of 100 μL by addition of 0.1% formic acid. To enrich the glycosylated fraction of tryptic peptides, solid phase extraction was performed using zwitterionic hydrophilic interaction liquid chromatography (ZIC-HILIC) in a pipette tip format (Protea Biosciences, Somerset, NJ, USA). Each ZIC-HILIC tip was wetted with water, equilibrated with 80% acetonitrile/0.1% formic acid, then loaded with a portion of the reconstituted digest in 80% acetonitrile (*i.e.*, 4 μL of reconstituted digest plus 16 μL acetonitrile). Each tip was then washed with 80% acetonitrile/0.1% formic acid. Finally, elution was performed using 0.1% formic acid.

Mass spectrometry

All analyses were conducted using a Synapt G2 HDMS quadrupole time of flight (Q-TOF) hybrid mass spectrometer (Waters, Manchester, UK). The instrument was fitted with a home-built static nanoflow electrospray ionization (nESI) stage which delivered the capillary potential by means of a platinum wire placed in contact with a small portion of analyte solution contained in a borosilicate emitter. Samples of approximately 10 μL purified digest or purified digest spiked to include 10 mM in imidazole (to enhance the abundance of lower charge states produced by nESI) were placed into nESI emitters using a 10 μL syringe (Hamilton, Reno, NV, USA). The emitters were fashioned in-house from 1.5–1.8 × 100 mm Corning Pyrex melting point capillaries (Corning, NY, USA) using a vertical micropipette pipette puller (David Kopf Instruments, Tujunga, CA, USA). Ionization by nESI was conducted using a capillary potential of 1.0–1.4 kV, a sampling cone voltage of 15–35 V, and an extraction cone voltage of 2–4 V. Source temperature was maintained at 80 °C. Precursor ions of interest were quadrupole selected and subjected to CID such that the trap region stacked ring ion guide of the instrument served as the collision cell. Argon was used as the collision gas at a pressure of approximately 5.0×10^{-3} mbar within the collision cell. Collision energy was modulated by adjusting the static DC offset (ΔU) between the collision cell and the stacked ring ion guide of the ion source region. Direct infusion spectra were acquired for approximately one minute.

Data handling

Spectrum acquisition and analysis was performed in MassLynx 4.1 (Waters), and further data processing and visualization were carried out using SigmaPlot 10.1 (Systat, Chicago, IL, USA) and using custom routines written and implemented in IGOR Pro 6.3 (WaveMetrics, Lake Oswego, OR, USA). Where practical, product ions resulting from cleavage of the carbohydrate group were assigned according to the nomenclature of Domon and Costello.[59] Occasionally, glycan fragmentations or combinations thereof could not be unambiguously or conveniently assigned using these formalisms. In such instances, the fragments were assigned by indicating monosaccharide losses from the precursor. Product ions involving scission of the peptide were assigned in accord with the nomenclature of Roepstorff and Fohlman.[60] When naming and referring to product ions, lower case letters were used to specify peptide fragmentation, while upper case letters were used to indicate oligosaccharide cleavage. For the sake of clarity, product ions resulting from small neutral losses (*e.g.*, H_2O, NH_3) from the precursor or other fragments were assigned but not labelled in the spectra presented below. Glycan structures were diagrammed using the monosaccharide symbology of Varki *et al.*[61] Peptide sequences were presented using standard one-letter amino acid notation, while monosaccharide names were abbreviated as follows: GlcNAc, *N*-acetylglucosamine; Man, mannose; Fuc, fucose; Xyl, xylose.

Results and discussion

CID of ECL glycopeptide ions

Upon nESI-MS analysis, the ZIC-HILIC purified tryptic digests of ECL yielded a major peak corresponding to the glycopeptide ion $[SKPAQGYGYLGVFNNSK + GlcNAc_2\ Man_3\ Fuc_1\ Xyl_1 + 3H]^{3+}$ (monoisotopic $m/z = 1000.8$). This glycopeptide was an attractive model analyte for our initial studies because, as discussed below, the MS/MS behavior of this analyte has been well-studied by others in the past (particularly, with respect to the complementarity of vibrational activation methods and electron capture/transfer methods for glycopeptide analysis). The ion was quadrupole selected and subjected to CID at a variety of collision energies. As shown in Fig. 1a and b, at a collision energy of $\Delta U = 17.5$ V the CID spectrum is dominated by Y-type glycosidic cleavages of the carbohydrate moiety. Sequential loss of individual monosaccharides occurred in various orders, ultimately resulting in a major fragment ion which corresponded to the $Y_{1\alpha} + Y_{1\beta}$ double cleavage product (*i.e.*, the peptide group plus a single remaining GlcNAc residue linked to the asparagine side chain). Not unexpectedly, the CID spectrum of this glycopeptide ion closely resembled the vibrational activation/dissociation spectra obtained by other researchers using IRMPD,[35] ion trap CID,[37] and beam-type CID in a Q-TOF.[38] It should be pointed out that the studies cited above were conducted on two variants of the target glycopeptide: one in which the residue two positions N-terminal of the glycosylation site was isoleucine, and another in which the isoleucine residue was replaced by a valine residue. Although this substitution of one aliphatic residue for another is unlikely to significantly affect the overall dissociation behavior of these glycopeptide variants, we note here that the present studies have been carried out using the valine-containing variant. In line with expectations, some very dissimilar CID results were obtained at somewhat higher collision energies. As depicted in Fig. 1c and d, at a collision energy of $\Delta U = 37.5$ V the spectrum changed dramatically in both overall appearance and in information content. Under these conditions, the base peak of the CID spectrum remained the $Y_{1\alpha} + Y_{1\beta}$ fragment, although a number of major ions in the spectrum were assigned as b- and y-type

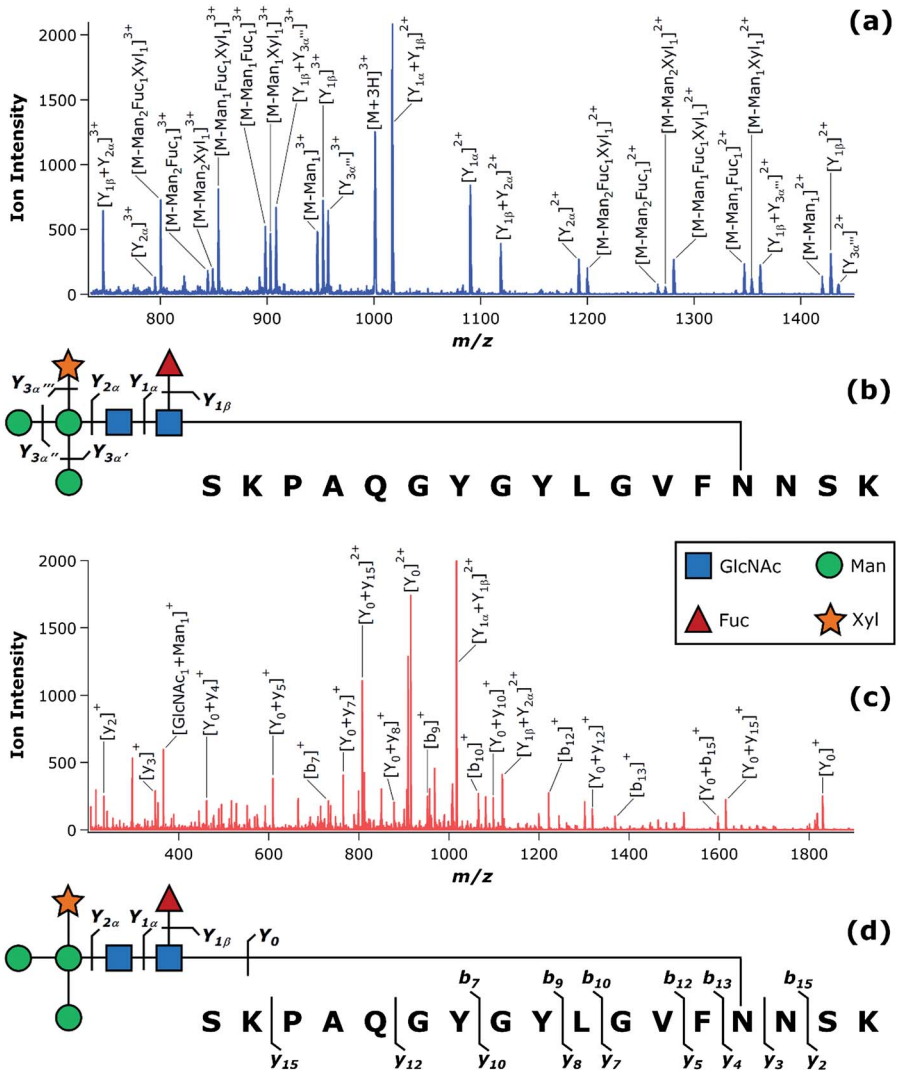

Fig. 1 CID of the triply protonated ECL glycopeptide. The CID spectrum acquired at $\Delta U = 17.5$ V (a) exhibited only glycan cleavage, as shown in the accompanying diagram (b). The CID spectrum acquired at $\Delta U = 37.5$ V (c) exhibited mainly peptide fragments following glycan loss, as shown in the accompanying diagram (d).

peptide sequence fragments. The observed product ions resulted in 56.3% sequence coverage for the peptide backbone, owing to six b ions and eight y ions representing cleavage of nine of the 16 peptide amide bonds. Notably, the CID sequence coverage reported here is quite reasonable when compared to those previously reported for this glycopeptide ion by ECD or ETD. Hakansson *et al.* obtained 68.8% sequence coverage by ECD (nine c ions and two z ions representing cleavage of 11 out of 16 N–C_α bonds),[35] while McLuckey and coworkers achieved 75.0% sequence coverage by ETD (11 c ions and 12 z ions representing cleavage of 12 out of 16 N–C_α bonds).[38]

To more completely delineate the energy-resolved CID behavior of this model glycopeptide, the peak areas of the $[M + 3H]^{3+}$ precursor ion and the corresponding product ions (or classes of product ions) were plotted as a function of ΔU (Fig. 2). As the collision energy was increased, the precursor ion was depleted and first yielded an assortment of Y_n glycan fragments, where $n > 1$. The relative proportion of these primary product ions crested at approximately $\Delta U = 17.5$ V, corresponding to the spectrum presented in Fig. 1a. Further increasing the collision energy resulted in diminished relative abundance of the $Y_{n>1}$ ions, with concomitant increase in proportion of Y_1 fragments, including $Y_{1\alpha}$, $Y_{1\beta}$, and the $Y_{1\alpha} + Y_{1\beta}$ double cleavage product. As the collision energy was elevated to $\Delta U > 32.5$ V, the continued diminution of $Y_{n>1}$ fragments was accompanied by declining abundance of Y_1 fragments. These reductions coincided with the production of a modest fraction of the Y_0 fragment (*i.e.*, loss of the entire oligosaccharide) and a substantial abundance of b- and y-type peptide fragments. This region of the energy-resolved CID plot corresponds to the spectrum given in Fig. 1c. At $\Delta U =$ 40.0 V, peptide b and y ions accounted for approximately 50% of the integrated peak area of the CID spectrum. Further increasing the collision energy led to loss of ion signal. Overall, these energy-resolved CID results confirm that, while only glycan fragments are yielded *via* the lowest energy dissociation pathways, significant information regarding the peptide

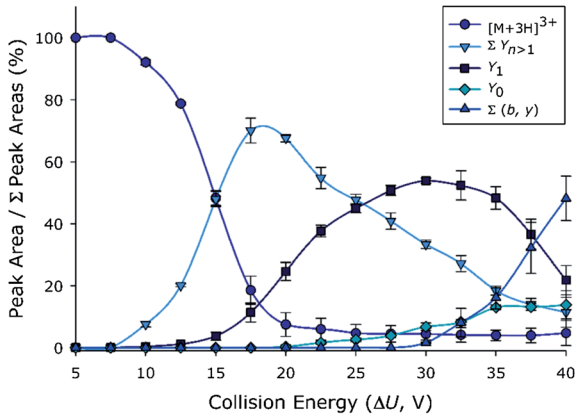

Fig. 2 Energy-resolved CID plot for the triply protonated ECL glycopeptide. The normalized peak area of each ion or group of ions is plotted as a function of the collision energy, expressed as the applied DC offset. Each data point represents the mean of four replicate measurements; error bars, where visible, represent the standard deviation.

sequence can be obtained as later generations of fragment ions evolve at higher collision energies.

Because the glycopeptide under investigation included two particularly basic sites (the ε amino groups of the two lysine residues), the triply protonated ion discussed above contains one readily mobile proton.[62,63] In order to evaluate how the absence of mobile protons would influence the dissociation channels of this model glycopeptide, the doubly protonated ion $[SKPAQGYGYLGVFNNSK + GlcNAc_2\ Man_3\ Fuc_1\ Xyl_1 + 2H]^{2+}$ (monoisotopic $m/z = 1500.7$) was generated by adding imidazole to the ZIC-HILIC enriched glycopeptide preparation. As illustrated in Fig. S1 of the ESI,† the $[M + 2H]^{2+}$ precursor ion also yielded CID spectra containing predominantly carbohydrate Y fragments (Fig. S1a and b†) at lower collision energies (in this example, $\Delta U = 47.5$ V), while relatively high collision energies (in this example, $\Delta U = 65.0$ V) brought about glycan loss with subsequent fragmentation of the polypeptide chain (Fig. S1c and d†). In comparing the product ion spectra of the $[M + 2H]^{2+}$ ion (*i.e.*, with only partially mobile protons) to those of the $[M + 3H]^{3+}$ ion (*i.e.*, with one readily mobile proton), it was found that, at appropriately chosen collision energies, the two precursors were able to yield much the same sequence information. The fragments providing the glycan connectivity were equivalently informative for both precursor ion charge states at the relatively low values of ΔU, and the same peptide sequence coverage was obtained at the relatively high values of ΔU. For the doubly charged precursor, the sequence coverage of 56.3% was obtained on the basis of six b ions and nine y ions.

Although the two charge states of this glycopeptide were able to supply similarly revealing CID spectra, not unexpectedly they did so at quite different settings of ΔU. The energy-resolved CID plot for the doubly charged precursor ion (Fig. S2 of the ESI†) was generated in the same manner as for the triply charged precursor ion. Although shifted to higher energies, the same general behavior was observed wherein $Y_{n>1}$ fragments of the oligosaccharide were the first fragments to appear, and as the collision energy was increased these fragments gave way to the Y_1 carbohydrate fragments followed by Y_0 glycan loss and finally b and y fragmentation of the peptide chain. It is important to note that the increases in ΔU values necessary to access the various fragmentation pathways was not solely due to differences in ion kinetic energy prior to collision. Applying a linear fit to the inflection point regions of the precursor ion survival curves allowed calculation of the ΔU values which corresponded to depletion of half the precursor ion signal. These 50% precursor ion survivals occurred at $\Delta U = 14.9$ V for the $[M + 3H]^{3+}$ glycopeptide ion and $\Delta U = 38.8$ V for the $[M + 2H]^{2+}$ precursor. The precursor ion kinetic energy (E_k) relates to the accelerating potential ΔU according to:

$$E_k = ze\Delta U \quad (1)$$

where z is the number of charges and e is the fundamental charge. The initial kinetic energies resulting in 50% precursor ion survival were therefore 44.7 eV for the $[M + 3H]^{3+}$ and 77.6 eV for the $[M + 2H]^{2+}$ ion. These observations are consistent with the mobile proton model, and serve to reiterate the critical importance of collision energy setting upon the information content of glycopeptide CID spectra, and how dramatically this dependence can vary depending on the charge state.

CID of BRB glycopeptide ions

In order to address whether the dissociation behaviors observed for the ECL glycopeptide might be generally true of other glycopeptides, another model analyte was selected for study. The ZIC-HILIC enriched BRB digest exhibited a number of glycopeptide ion signals on nESI-MS analysis. The various peaks represented the microheterogeneity of the BRB glycosylation site, as well as an assortment of fully and partially tryptic digestion products. Among the most abundant signals was the glycopeptide ion $[SRNLTK + GlcNAc_2\ Man_5 + 2H]^{2+}$ (monoisotopic $m/z = 968.6$). This model glycopeptide serves as an interesting contrast to the ECL glycopeptide, in that they harbor different classes of N-glycans (paucimannosidic in the case of the ECL glycopeptide; high mannose in the case of BRB) and have polypeptide groups of quite different lengths (17 amino acid residues in the case of the ECL glycopeptide; six in the case of the BRB glycopeptide). CID spectra of the $[M + 2H]^{2+}$ BRB glycopeptide ion are provided in Fig. 3. Much as was noted for the ECL glycopeptide, at relatively low collision energy only the glycan was cleaved (Fig. 3a and b). Conducting CID at $\Delta U = 30.0$ V generated a complete series of Y-type oligosaccharide fragmentation products, which provided the complete glycan composition for this glycopeptide. This spectrum presented in Fig. 3a was found to be less complex than the analogous spectrum of the ECL glycopeptide (Fig. 1a) owing to the lesser number of monosaccharide masses involved, and the correspondingly fewer possible product ion masses arising from oligosaccharide fragmentation. When CID was performed at $\Delta U = 55.0$ V, the dissociation spectrum became dominated by peptide fragments (Fig. 3c and d). These higher energy dissociation pathways yielded product ions covering 80% of the peptide sequence (three b ions and two y ion representing

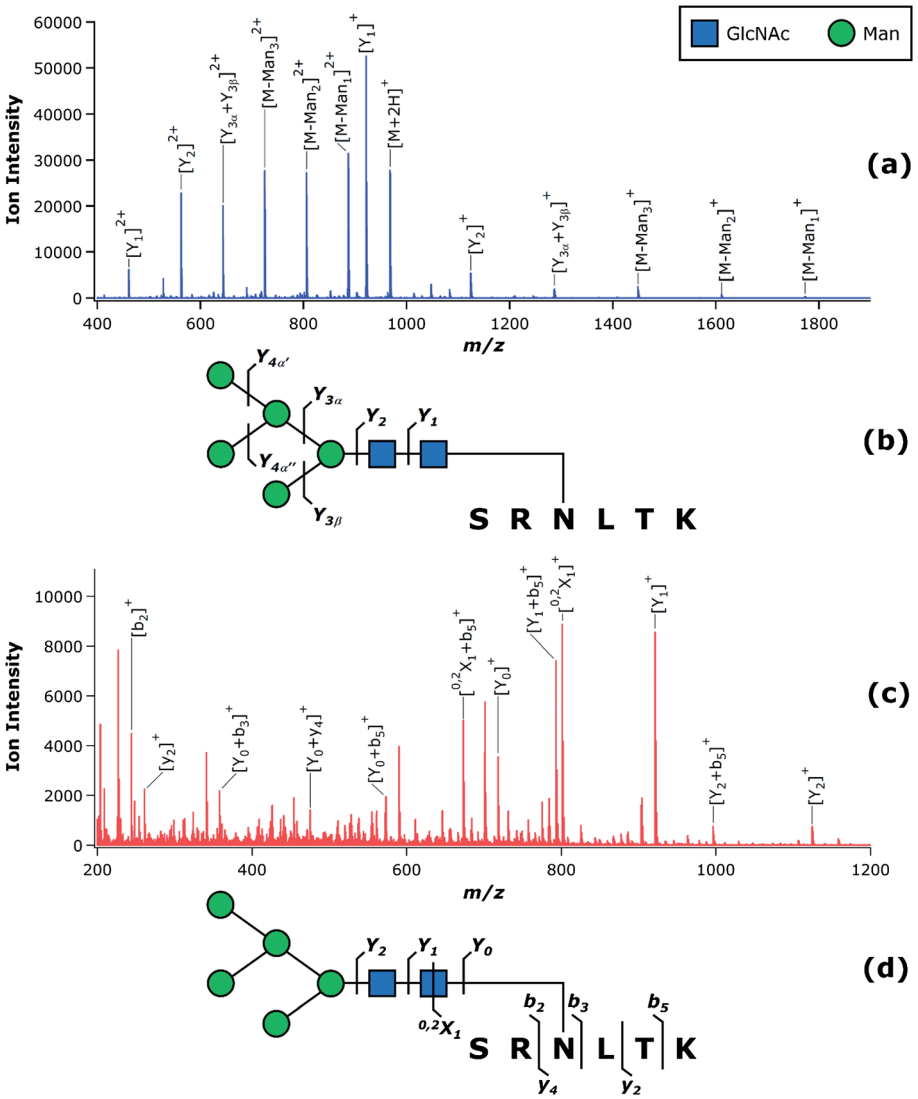

Fig. 3 CID of the doubly protonated BRB glycopeptide. The CID spectrum acquired at $\Delta U = 30.0$ V (a) exhibited only glycan cleavage, as shown in the accompanying diagram (b). The CID spectrum acquired at $\Delta U = 55.0$ V (c) exhibited mainly peptide fragments following glycan loss, as shown in the accompanying diagram (d).

cleavage of four out of five peptide amide bonds). These observations reinforce the findings for the ECL glycopeptide, where CID spectra alternately produced glycan fragmentation or peptide fragmentation depending on the applied collision energies. In one contrast to the ECL glycopeptide, at elevated collision energies the BRB glycopeptide was found to yield cross-ring cleavage of the terminal GlcNAc residue ($^{0,2}X_1$). Furthermore, the BRB glycopeptide exhibited some examples of peptide fragmentation without complete loss of the glycan. For instance, the $^{0,2}X_1 + b_5$ and $Y_1 + b_5$ internal fragments were among the most abundant signals in the $\Delta U = 55.0$ V CID spectrum (Fig. 3c). This highlights the possibility that glycan and peptide dissociation channels may take place concurrently under certain circumstances (*e.g.*, when a particularly favored peptide backbone cleavage is available). Similar findings have previously been noted in vibrational activation/dissociation of O-glycopeptides containing proline residues.[27,64] In those instances, the proline effect[65–67] rendered peptide fragmentation competitive with glycan loss.

The energy-resolved CID behavior of the doubly protonated BRB glycopeptide is presented in Fig. 4. On comparison to the triply protonated ECL glycopeptide ion (Fig. 2), the onset of dissociation for the triply protonated BRB glycopeptide occurred at somewhat higher collision energies, with the 50% precursor ion survival being reached at $\Delta U = 26.2$ V (corresponding to $E_k = 52.4$ eV) for the $[M + 2H]^{2+}$ BRB glycopeptide, as compared to $\Delta U = 14.9$ V (corresponding to $E_k = 44.7$ eV) for the $[M + 3H]^{3+}$ ECL glycopeptide. Such differences were not unexpected, given the presence of a readily mobile proton in the case of the triply protonated ECL glycopeptide ion, and the availability of only partially mobile protons in the case of the doubly protonated BRB glycopeptide ion. It should be noted that the substantially different molecular weights of the two glycopeptides (monoisotopic mass of 2999.3 u for the ECL glycopeptide; 1936.2 u for

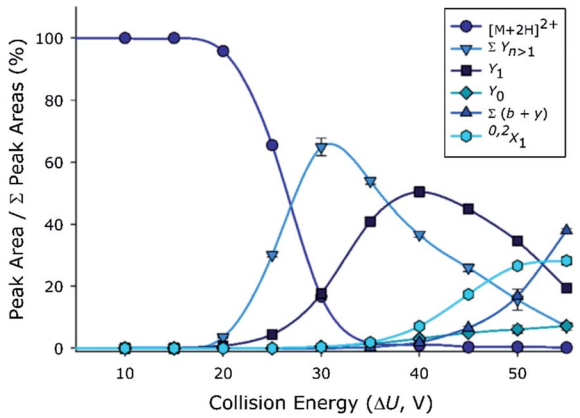

Fig. 4 Energy-resolved CID plot for the doubly protonated BRB glycopeptide. The normalized peak area of each ion or group of ions is plotted as a function of the collision energy, expressed as the applied DC offset. Each data point represents the mean of three replicate measurements; error bars, where visible, represent the standard deviation.

the BRB glycopeptide) and the commensurate disparity in their vibrational degrees of freedom also contributes to quantitative differences in the energy-resolved CID behavior. Aside from the absolute collision energies at which different kinds of dissociation pathways were accessed, the two sets of energy-resolved CID data were in strong agreement regarding the initial appearance of $Y_{n>1}$ glycan fragments followed by Y_1 glycan fragments, which in turn ultimately yielded Y_0 fragment ions (complete glycan loss) and peptide b and y fragment ions. Interestingly, the energy dependences of various dissociation pathways qualitatively mirrored those of the ECL glycopeptide ions. Indeed, these energy-resolved CID data were in strong concordance regarding the initial appearance of $Y_{n>1}$ glycan fragments followed by Y_1 glycan fragments, which in turn ultimately yielded Y_0 fragment ions (complete glycan loss) and peptide b and y fragment ions. These qualitative similarities in the energy-dependent dissociation behavior is rather remarkable, given the significant differences between the glycopeptides in terms of structure and composition.

To again probe the influence of proton mobility on the information content of the CID spectra, the [SRNLTK + $GlcNAc_2Man_5$ + $3H]^{3+}$ (monoisotopic m/z = 645.7) ion was next studied. This ion was observed along with the corresponding doubly charged ion upon nESI-MS analysis of the purified BRB digest, although in less abundance. In contrast to the BRB $[M + 2H]^{2+}$ ion, this BRB $[M + 3H]^{3+}$ ion has a number of ionizing protons which exceeds the number of basic amino acid side chains, and thus has a readily mobile proton. As illustrated in Fig. S3 of the ESI,† CID at $\Delta U = 10.0$ V produced only Y-type glycan fragments (Fig. S3a and b†), while at $\Delta U = 40.0$ V peptide b and y ions were observed (Fig. S3c and d†). The product ions arising from polypeptide cleavage provided 60% sequence coverage (three b ions and one y ion representing cleavage of three out of five peptide bonds). Predictably, the energy-resolved CID plot for the triply protonated BRB precursor ion exhibited lower dissociation onset energies as compared to the doubly protonated precursor, owing to both the differing charge states (and thus different dependence of E_k upon ΔU) as well as the differences in proton mobility (Fig. S4 of the ESI†). These considerations notwithstanding, the general observation that glycan connectivity and peptide sequence can be differentially accessed at different collision energies again held true for this precursor ion.

Multi-energy CID of the ECL and BRB glycopeptides

The energy-resolved CID data discussed above served to suggest the intriguing possibility of capturing oligosaccharide and polypeptide sequence information in a single mass spectrum. In order to achieve this, online collision energy modulation was applied during direct infusion acquisition of CID spectra in order to sample informative dissociation channels of different

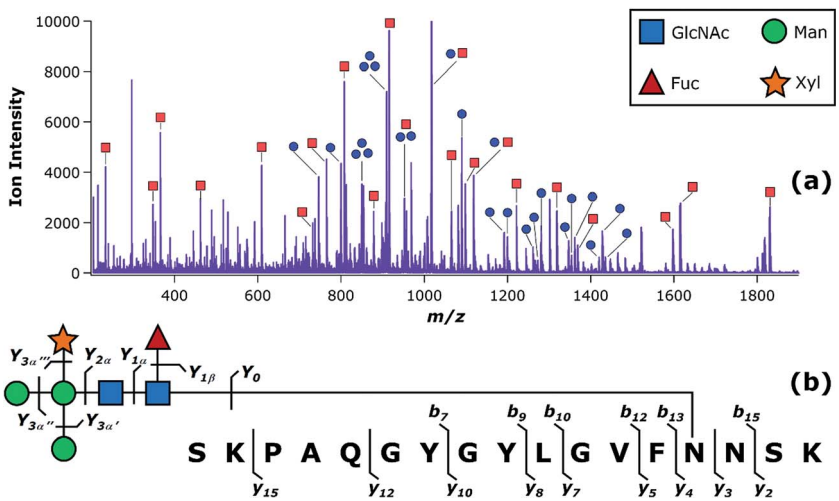

Fig. 5 Multi-energy CID of the triply protonated ECL glycopeptide. The CID spectrum (a) was acquired *via* online switching between two collision energies: ΔU = 17.5 V and ΔU = 37.5 V. These correspond to the collision energies applied in Fig. 1a and c, respectively. Peak assignments are the same as those shown in Fig. 1a (labeled here with blue circles) and Fig. 1c (labeled here with red squares). An abundance of both glycan and peptide fragments were observed, as shown in the accompanying diagram (b).

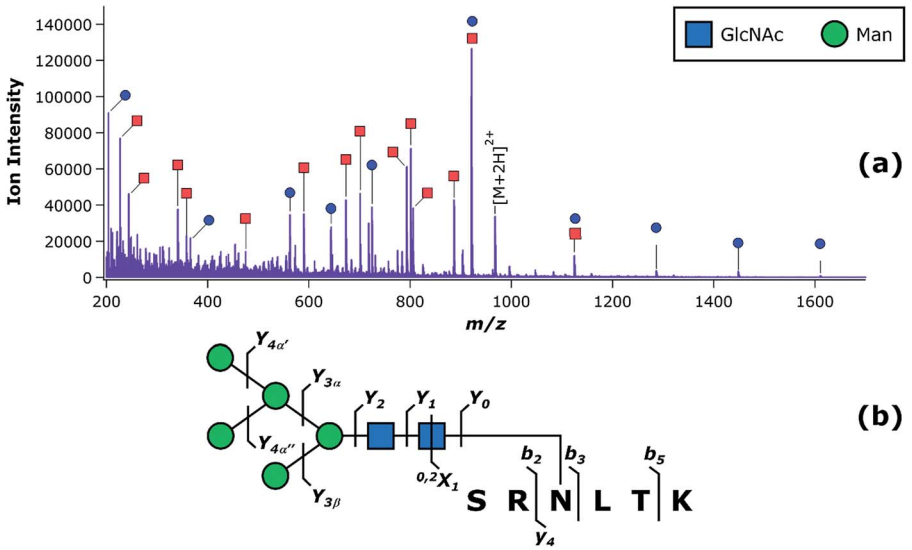

Fig. 6 Multi-energy CID of the doubly protonated BRB glycopeptide. The CID spectrum (a) was acquired *via* online switching between two collision energies: $\Delta U = 30.0$ V and $\Delta U = 55.0$ V. These correspond to the collision energies applied in Fig. 3a and c, respectively. Peak assignments are the same as those shown in Fig. 3a (labeled here with blue circles) and Fig. 3c (labeled here with red squares). An abundance of both glycan and peptide fragments were observed, as shown in the accompanying diagram (b).

energetic requirements. The multi-energy CID spectrum of the $[M + 3H]^{3+}$ ECL glycopeptide ion is presented in Fig. 5. The spectrum exhibited a wealth of product ions which collectively resulted in complete coverage of the glycan Y-type ions and 56% peptide sequence coverage (six b ions and nine y ions accounting for scission of nine of the 16 peptide amide bonds). The multi-energy CID spectrum for the $[M + 2H]^{2+}$ ECL glycopeptide ion (Fig. S5 of the ESI†) provided essentially the same information content. Also noteworthy is that the multi-energy CID spectra obtained through online collision energy modulation compare favorably to the dissociation spectra obtained at a single collision energy (*cf.* Fig. 1b and d, and Fig. 5b). Similarly, multi-energy CID of the $[M + 2H]^{2+}$ BRB glycopeptide (Fig. 6) was revealing of a complete series of Y-type glycosidic cleavages as well as 80% coverage of the peptide sequence coverage (three b ions and two y ions accounting for scission of four of the five peptide amide bonds). Again, comparable connectivity information was obtained upon multi-energy CID analysis of an alternative charge state of the analyte (in this case, the $[M + 3H]^{3+}$ BRB glycopeptide ion; Fig. S6 of the ESI†). Furthermore, the multi-energy CID results for the BRB glycopeptide were found to be of approximately equivalent information content as was achieved in the individual, static collision energy spectra (*cf.*, Fig. 3b, d, and Fig. 6b). Overall, the modulation of collision energy without interrupting spectrum acquisition was found to be a viable approach to obtaining highly informative CID spectra which address the structures of both the glycan and peptide moieties.

Conclusions

Although vibrational activation/dissociation MS/MS methods are perhaps best known for the ability to provide information on the carbohydrate moiety of glycopeptides, these data underscore and extend previous observations that, at appropriately chosen collision energies, substantial peptide sequence information can be obtained *via* low-energy beam-type CID. This was found to be true of four model glycopeptide ions which were quite dissimilar in a number of other respects (glycan type and composition; peptide size and composition), and were each investigated as protonated ions having charge states that provided differing proton mobilities. Despite these variables, the analyte ions studied herein adhered to strikingly similar energy-resolved CID behaviors from a qualitative standpoint. In each case, $Y_{n>1}$ carbohydrate cleavage was observed as the lowest-energy, first generation dissociation pathway. With increasing collision energy, production of the Y_1 glycan fragment was observed, which in turn gave rise to the Y_0 product along with b and y ions. Based on the energy-resolved CID precursor and product ion abundance curves, the peptide b and y ions appear to be tertiary fragments which, accordingly, have much higher appearance energy thresholds as compared to the glycan-related scissions. Our findings in aggregate serve to suggest that these dissociation behaviors may be quite general among a diverse range of glycosylated peptides bearing different glycan classes and various peptide characteristics.

The higher energy required to access peptide-informative dissociation channels may in part explain why such ions are sometimes not observed. For example, low-energy CID in an ion trap would not be expected to yield consecutive fragmentation in single MS/MS experiment, since this method only imparts translational energy to the precursor ion. Likewise, IRMPD may in some cases be too slow an activation process to provide extensive peptide sequence information, even though IRMPD is in principle capable of accessing consecutive dissociation products. Although the present findings may be of less

usefulness in conjunction with these "slow heating"[68] vibrational activation methods, they can be of immediate analytical utility when analysis is carried out using any low-energy, beam-type CID instrument, such as tandem quadrupoles, quadrupole time-of-flight hybrids, and various other hybrid mass spectrometers which enable beam-type collisional activation. This includes "higher-energy collisional dissociation" (HCD), which is merely a vendor-specific implementation and terminology for low-energy beam-type CID.

While qualitatively quite similar, there were some important quantitative differences in the energy-resolved CID data among the model glycopeptide ions investigated here. Clearly, the composition, charge state, and proton mobility of the precursor ion exert great influence on the absolute collision energies at which various classes of dissociation products are observed. Accordingly, the ability to collect both glycan and peptide information in a multi-energy CID spectrum hinges upon appropriate selection of the applied ΔU values. Thus, further study of the energy dependence of glycopeptide fragmentation pathways seems warranted. In this respect, some theoretical progress has been made towards predicting glycopeptide tandem mass spectra on the basis of a kinetic model; however, thus far this has only been performed from the standpoint of ion trap CID under conditions which would not be expected to lead to peptide sequence information.[69] We are currently pursuing this line of inquiry from an experimental standpoint. Based on energy-resolved CID studies of families of glycopeptides with key differences in composition and charge state, we find that the general conclusions of the present study extend to numerous other glycopeptide analytes, and further that it may be possible to predict collision energies that result in specific fragment types (indeed, the charge state and degrees of freedom corrected 50% precursor ion survival energies seem to correlate well with proton mobility, as summarized in Table S1 of the ESI†).

Finally, we note that the development of an enhanced understanding of how CID yields peptide information is quite significant given that the alternatives for this task – ECD and ETD – are not as widely available on as eclectic an array of MS instruments as compared to CID. Thus, there is potential for substantial impact of these findings in the context of glycoproteomics. The major advantage of ETD is that the peptide backbone can be fragmented without elimination of the glycan, thus allowing unambiguous and direct assignment of the site of modification. However, in many cases involving N-glycosylation, loss of the glycan does not preclude site localization owing to the specificity of N-glycan attachment to only asparagine residues within the context of NXT or NXT consensus sequon (where X is any amino acid residue except proline). For tryptic N-glycopeptides which contain only one potential N-glycosylation site, glycan loss at the stage of MS/MS does not pose a significant limitation for site localization. Moreover, we note that modulating ΔU values to capture spectra at different collision energies can be done in a matter of a few milliseconds, making this approach at least as fast (and potentially faster) than online switching to ETD. This presents an advantage from the standpoint of sampling LC-MS peaks. Overall, these results indicate the possibility of some generally applicable principles of energy-resolved glycopeptide ion CID behaviors of glycosylated peptide ions, while concomitantly underscoring the need for further study of the absolute collision energies necessary to access desired types of fragmentation information. The accomplishment of these goals would undoubtedly bring considerable analytical benefits to the field of glycoproteomics with regards to maximizing the structural information content of glycopeptide CID spectra.

Acknowledgements

Funding from the University of Nebraska, which was provided in part by the Nebraska Tobacco Settlement Biomedical Research Development Fund, is gratefully acknowledged.

References

1 D. S. Dalpathado and H. Desaire, *Analyst*, 2008, **133**, 731–738.
2 H. J. An, J. W. Froehlich and C. B. Lebrilla, *Curr. Opin. Chem. Biol.*, 2009, **13**, 421–426.
3 B. Tissot, S. J. North, A. Ceroni, P.-C. Pang, M. Panico, F. Rosati, A. Capone, S. M. Haslam, A. Dell and H. R. Morris, *FEBS Lett.*, 2009, **583**, 1728–1735.
4 J. E. Schiel, *Anal. Bioanal. Chem.*, 2012, **404**, 1141–1149.
5 H. Desaire, *Mol. Cell. Proteomics*, 2013, **12**, 893–901.
6 A. Varki, *Glycobiology*, 1993, **3**, 97–130.
7 R. A. Dwek, *Chem. Rev.*, 1996, **96**, 683–720.
8 K. Ohtsubo and J. D. Marth, *Cell*, 2006, **126**, 855–867.
9 E. Marklova and Z. Albahri, *Clin. Chim. Acta*, 2007, **385**, 6–20.
10 H. J. An, S. R. Kronewitter, M. L. A. de Leoz and C. B. Lebrilla, *Curr. Opin. Chem. Biol.*, 2009, **13**, 601–607.
11 H. Schachter and H. H. Freeze, *Biochim. Biophys. Acta*, 2009, **1792**, 925–930.
12 H. Hwang, J. Zhang, K. A. Chung, J. B. Leverenz, C. P. Zabetian, E. R. Peskind, J. Jankovic, Z. Su, A. M. Hancock, C. Pan, T. J. Montine, S. Pan, J. Nutt, R. Albin, M. Gearing, R. P. Beyer, M. Shi and J. Zhang, *Mass Spectrom. Rev.*, 2010, **29**, 79–125.
13 L. Sturiale, R. Barone and D. Garozzo, *J. Inherited Metab. Dis.*, 2011, **34**, 891–899.
14 B. Adamczyk, T. Tharmalingam and P. M. Rudd, *Biochim. Biophys. Acta*, 2012, **1820**, 1347–1353.
15 D. Kolarich, B. Lepenies and P. H. Seeberger, *Curr. Opin. Chem. Biol.*, 2012, **16**, 214–220.
16 L. S. C. Kreisman and B. A. Cobb, *Glycobiology*, 2012, **22**, 1019–1030.
17 H. H. Freeze, *J. Biol. Chem.*, 2013, **288**, 6936–6945.
18 E. D. Dodds, R. R. Seipert, B. H. Clowers, J. B. German and C. B. Lebrilla, *J. Proteome Res.*, 2009, **8**, 502–512.
19 M. Wuhrer, A. M. Deelder and C. H. Hokke, *J. Chromatogr. B: Anal. Technol. Biomed. Life Sci.*, 2005, **825**, 124–133.
20 W. Morelle, K. Canis, F. Chirat, V. Faid and J. C. Michalski, *Proteomics*, 2006, **6**, 3993–4015.
21 W. Morelle and J. C. Michalski, *Nat. Protoc.*, 2007, **2**, 1585–1602.

22 B. H. Clowers, E. D. Dodds, R. R. Seipert and C. B. Lebrilla, *J. Proteome Res.*, 2007, **6**, 4032–4040.
23 J. W. Froehlich, E. D. Dodds, M. Wilhelm, O. Serang, J. A. Steen and R. S. Lee, *Mol. Cell. Proteomics*, 2013, **12**, 1017–1025.
24 J. W. Froehlich, M. Barboza, C. Chu, L. A. Lerno, Jr, B. H. Clowers, A. M. Zivkovic, J. B. German and C. B. Lebrilla, *Anal. Chem.*, 2011, **83**, 5541–5547.
25 K. Vekey, O. Ozohanics, E. Toth, A. Jeko, A. Revesz, J. Krenyacz and L. Drahos, *Int. J. Mass Spectrom.*, 2013, **345–347**, 71–79.
26 R. R. Seipert, E. D. Dodds, B. H. Clowers, S. M. Beecroft, J. B. German and C. B. Lebrilla, *Anal. Chem.*, 2008, **80**, 3684–3692.
27 R. R. Seipert, E. D. Dodds and C. B. Lebrilla, *J. Proteome Res.*, 2009, **8**, 493–501.
28 Y. Yoshimura, T. Matsushita, N. Fujitani, Y. Takegawa, H. Fujihira, K. Naruchi, X.-D. Gao, N. Manri, T. Sakamoto, K. Kato, H. Hinou and S.-I. Nishimura, *Biochemistry*, 2010, **49**, 5929–5941.
29 N. Manri, H. Satake, A. Kaneko, A. Hirabayashi, T. Baba and T. Sakamoto, *Anal. Chem.*, 2013, **85**, 2056–2063.
30 Z. Zhu, D. Hua, D. F. Clark, E. P. Go and H. Desaire, *Anal. Chem.*, 2013, **85**, 5023–5032.
31 Z. Zhu, X. Su, D. F. Clark, E. P. Go and H. Desaire, *Anal. Chem.*, 2013, **85**, 8403–8411.
32 L. Zhang and J. P. Reilly, *J. Proteome Res.*, 2008, **8**, 734–742.
33 J. A. Madsen, B. J. Ko, H. Xu, J. A. Iwashkiw, S. A. Robotham, J. B. Shaw, M. F. Feldman and J. S. Brodbelt, *Anal. Chem.*, 2013, **85**, 9253–9261.
34 E. Mirgorodskaya, P. Roepstorff and R. A. Zubarev, *Anal. Chem.*, 1999, **71**, 4431–4436.
35 K. Hakansson, H. J. Cooper, M. R. Emmett, C. E. Costello, A. G. Marshall and C. L. Nilsson, *Anal. Chem.*, 2001, **73**, 4530–4536.
36 K. Hakansson, M. J. Chalmers, J. P. Quinn, M. A. McFarland, C. L. Hendrickson and A. G. Marshall, *Anal. Chem.*, 2003, **75**, 3256–3262.
37 J. M. Hogan, S. J. Pitteri, P. A. Chrisman and S. A. McLuckey, *J. Proteome Res.*, 2005, **4**, 628–632.
38 H. Han, Y. Xia, M. Yang and S. A. McLuckey, *Anal. Chem.*, 2008, **80**, 3492–3497.
39 A. Halim, J. Nilsson, U. Ruetschi, C. Hesse and G. Larson, *Mol. Cell. Proteomics*, 2012, **11**, 1–17.
40 A. Halim, U. Ruetschi, G. Larson and J. Nilsson, *J. Proteome Res.*, 2013, **12**, 573–584.
41 C. Singh, C. G. Zampronio, A. J. Creese and H. J. Cooper, *J. Proteome Res.*, 2012, **11**, 4517–4525.
42 D. Wang, M. Hincapie, T. Rejtar and B. L. Karger, *Anal. Chem.*, 2011, **83**, 2029–2037.
43 H. Ye, M. T. Boyne, L. F. Buhse and J. Hill, *Anal. Chem.*, 2013, **85**, 1531–1539.
44 M. Wuhrer, M. I. Catalina, A. M. Deelder and C. H. Hokke, *J. Chromatogr. B: Anal. Technol. Biomed. Life Sci.*, 2007, **849**, 115–128.
45 J. Zaia, *Omics*, 2010, **14**, 401–418.
46 E. D. Dodds, *Mass Spectrom. Rev.*, 2012, **31**, 666–682.
47 W. R. Alley, Jr, B. F. Mann and M. V. Novotny, *Chem. Rev.*, 2013, **113**, 2668–2732.
48 J. T. Adamson and K. Hakansson, *J. Proteome Res.*, 2006, **5**, 493–501.
49 L. Bindila, K. Steiner, C. Schaffer, P. Messner, M. Mormann and J. Peter-Katalinic, *Anal. Chem.*, 2007, **79**, 3271–3279.
50 N. V. Bykova, C. Rampitsch, O. Krokhin, K. G. Standing and W. Ens, *Anal. Chem.*, 2006, **78**, 1093–1103.
51 C. W. Damen, W. Chen, A. B. Chakraborty, M. van Oosterhout, J. R. Mazzeo, J. C. Gebler, J. H. Schellens, H. Rosing and J. H. Beijnen, *J. Am. Soc. Mass Spectrom.*, 2009, **20**, 2021–2033.
52 O. Krokhin, W. Ens, K. G. Standing, J. Wilkins and H. Perreault, *Rapid Commun. Mass Spectrom.*, 2004, **18**, 2020–2030.
53 Z. M. Segu and Y. Mechref, *Rapid Commun. Mass Spectrom.*, 2010, **24**, 1217–1225.
54 N. E. Scott, B. L. Parker, A. M. Connolly, J. Paulech, A. V. G. Edwards, B. Crossett, L. Falconer, D. Kolarich, S. P. Djordjevic, P. Hojrup, N. H. Packer, M. R. Larsen and S. J. Cordwell, *Mol. Cell. Proteomics*, 2011, **10**, 1–18.
55 J. Irungu, E. P. Go, Y. Zhang, D. S. Dalpathado, H. X. Liao, B. F. Haynes and H. Desaire, *J. Am. Soc. Mass Spectrom.*, 2008, **19**, 1209–1220.
56 F. Jahouh, S. J. Hou, P. Kovac and J. H. Banoub, *J. Mass Spectrom.*, 2011, **46**, 993–1003.
57 V. Franc, M. Sebela, P. Rehulka, R. Koncitikova, R. Lenobel, C. Madzak and D. Kopecny, *J. Proteomics*, 2012, **75**, 4027–4037.
58 M. Tajiri, M. Kadoya and Y. Wada, *J. Proteome Res.*, 2009, **8**, 688–693.
59 B. Domon and C. E. Costello, *Glycoconjugate J.*, 1988, **5**, 397–409.
60 P. Roepstorff and J. Fohlman, *Biomed. Mass Spectrom.*, 1984, **11**, 601.
61 A. Varki, R. D. Cummings, J. D. Esko, H. H. Freeze, P. Stanley, J. D. Marth, C. R. Bertozzi, G. W. Hart and M. E. Etzler, *Proteomics*, 2009, **9**, 5398–5399.
62 A. R. Dongre, J. L. Jones, A. Somogyi and V. H. Wysocki, *J. Am. Chem. Soc.*, 1996, **118**, 8365–8374.
63 V. H. Wysocki, G. Tsaprailis, L. L. Smith and L. A. Breci, *J. Mass Spectrom.*, 2000, **35**, 1399–1406.
64 I. Perdivara, L. Perera, M. Sricholpech, M. Terajima, N. Pleshko, M. Yamauchi and K. B. Tomer, *J. Am. Soc. Mass Spectrom.*, 2013, **24**, 1072–1081.
65 L. A. Breci, D. L. Tabb, J. R. Yates and V. H. Wysocki, *Anal. Chem.*, 2003, **75**, 1963–1971.
66 B. Paizs and S. Suhai, *Mass Spectrom. Rev.*, 2005, **24**, 508–548.
67 Y. Huang, G. C. Tseng, S. Yuan, L. Pasa-Tolic, M. S. Lipton, R. D. Smith and V. H. Wysocki, *J. Proteome Res.*, 2008, **7**, 70–79.
68 S. A. McLuckey and D. E. Goeringer, *J. Mass Spectrom.*, 1997, **32**, 461–474.
69 Z. Zhang and B. Shah, *Anal. Chem.*, 2010, **82**, 10194–10202.

Electronic Supplementary Material (ESI) for Analyst.

Supplementary Data to Accompany:

Energy-Resolved Collision-Induced Dissociation Pathways of Model N-Linked Glycopeptides: Implications for Capturing Glycan Connectivity and Peptide Sequence in a Single Experiment

Venkata Kolli and Eric D. Dodds

Department of Chemistry, University of Nebraska – Lincoln

Lincoln, NE 68588-0304 USA

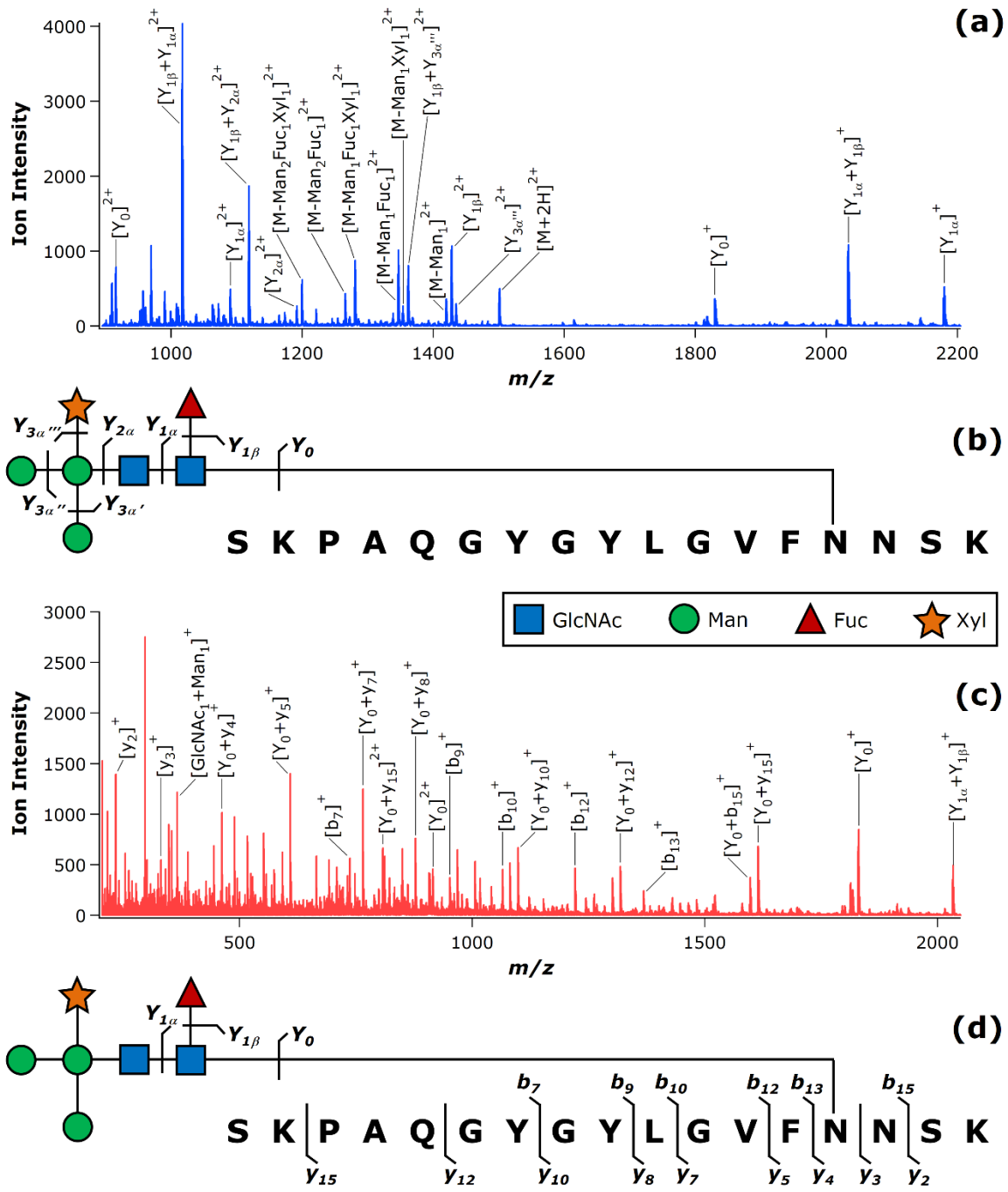

Figure S1. CID of the doubly protonated ECL glycopeptide. The CID spectrum acquired at ΔU = 47.5 V **(a)** exhibited only glycan cleavage, as shown in the accompanying diagram **(b)**. The CID spectrum acquired at ΔU = 65.0 V **(c)** exhibited mainly peptide fragments following glycan loss, as shown in the accompanying diagram **(d)**.

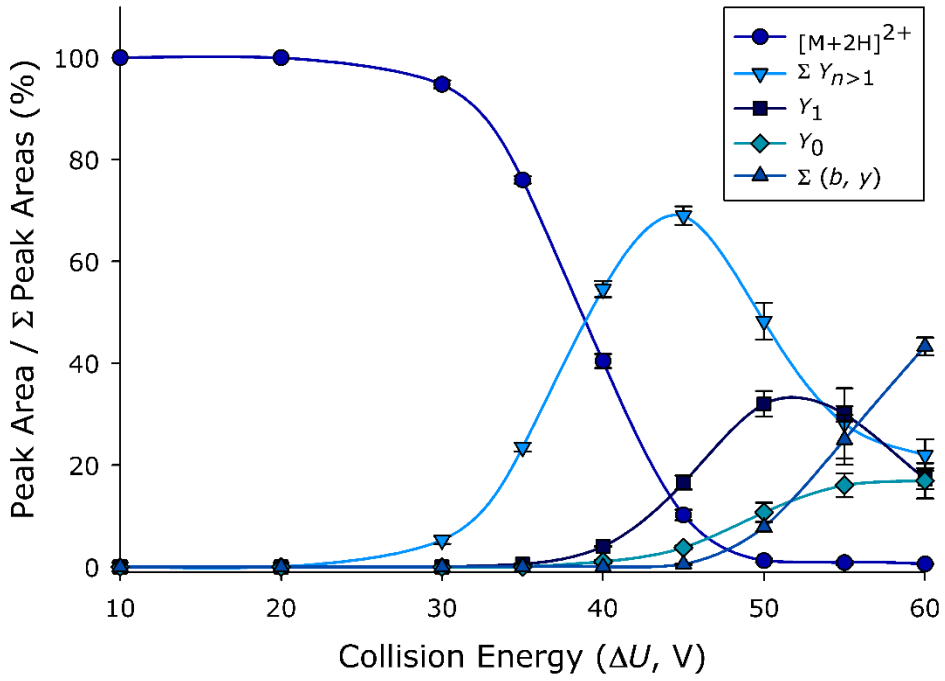

Figure S2. Energy-resolved CID plot for the doubly protonated ECL glycopeptide. The normalized peak area of each ion or group of ions is plotted as a function of the collision energy, expressed as the applied DC offset. Each data point represents the mean of three replicate measurements; error bars, where visible, represent the standard deviation.

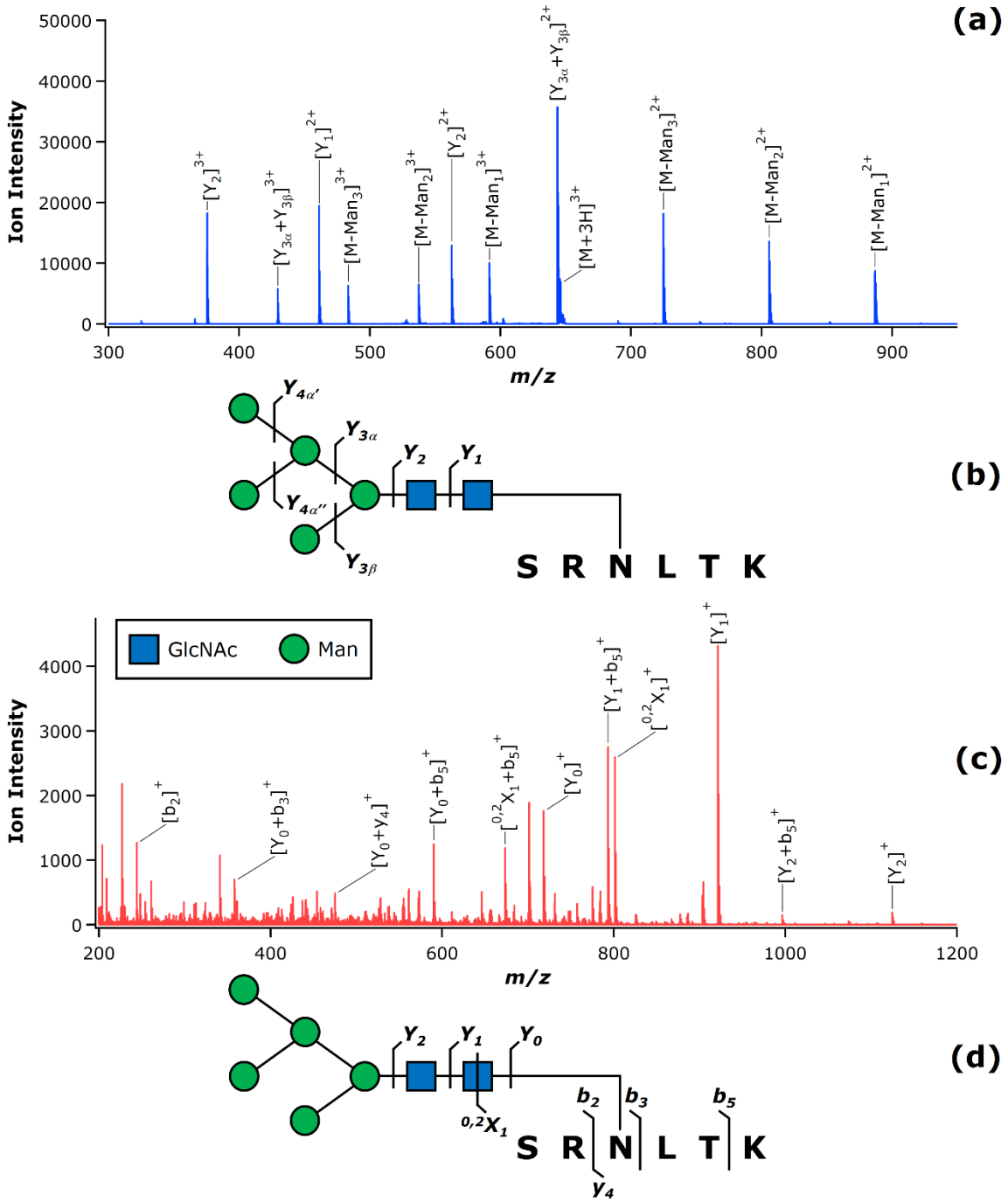

Figure S3. CID of the triply protonated BRB glycopeptide. The CID spectrum acquired at ΔU = 10.0 V **(a)** exhibited only glycan cleavage, as shown in the accompanying diagram **(b)**. The CID spectrum acquired at ΔU = 40.0 V **(c)** exhibited mainly peptide fragments following glycan loss, as shown in the accompanying diagram **(d)**.

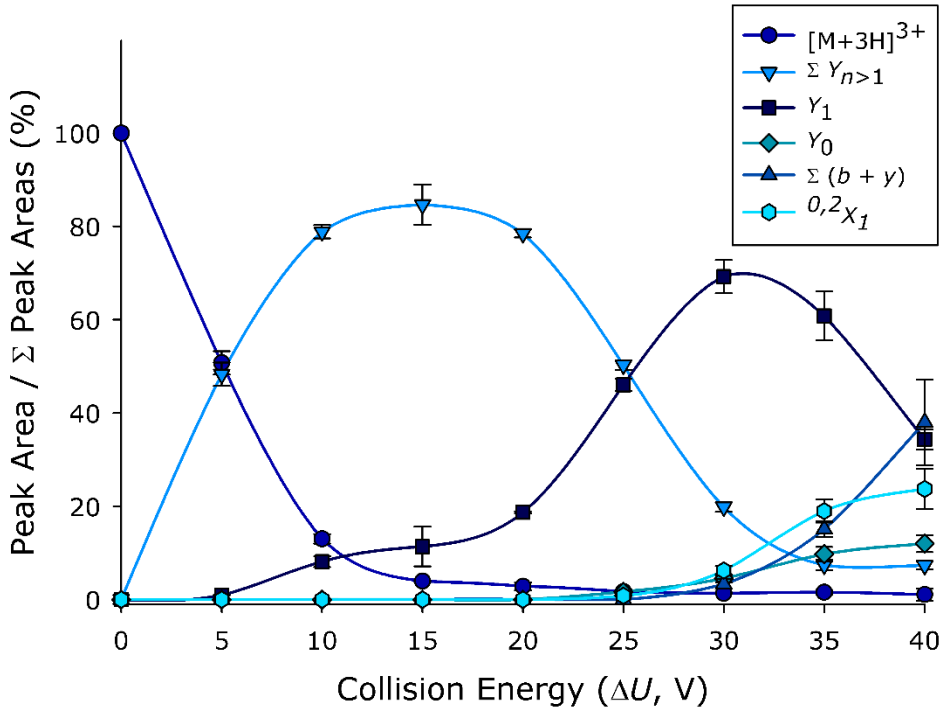

Figure S4. Energy-resolved CID plot for the triply protonated BRB glycopeptide. The normalized peak area of each ion or group of ions is plotted as a function of the collision energy, expressed as the applied DC offset. Each data point represents the mean of three replicate measurements; error bars, where visible, represent the standard deviation.

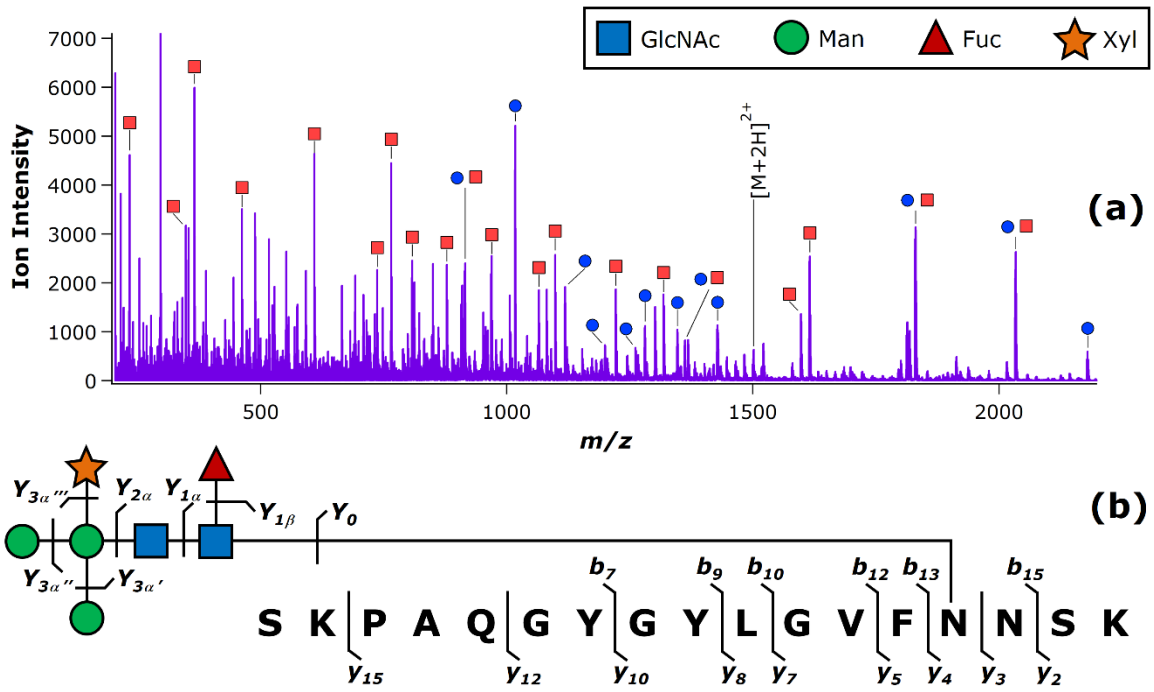

Figure S5. Multi-energy CID of the doubly protonated ECL glycopeptide. The CID spectrum **(a)** was acquired via online switching between two collision energies: ΔU = 47.5 V and ΔU = 65.0 V. These correspond to the collision energies applied in **Figure S1a** and **Figure S1c**, respectively. Peak assignments are the same as those shown in **Figure S1a** (labeled here with blue circles) and **Figure S1c** (labeled here with red squares). An abundance of both glycan and peptide fragments were observed, as shown in the accompanying diagram **(b)**.

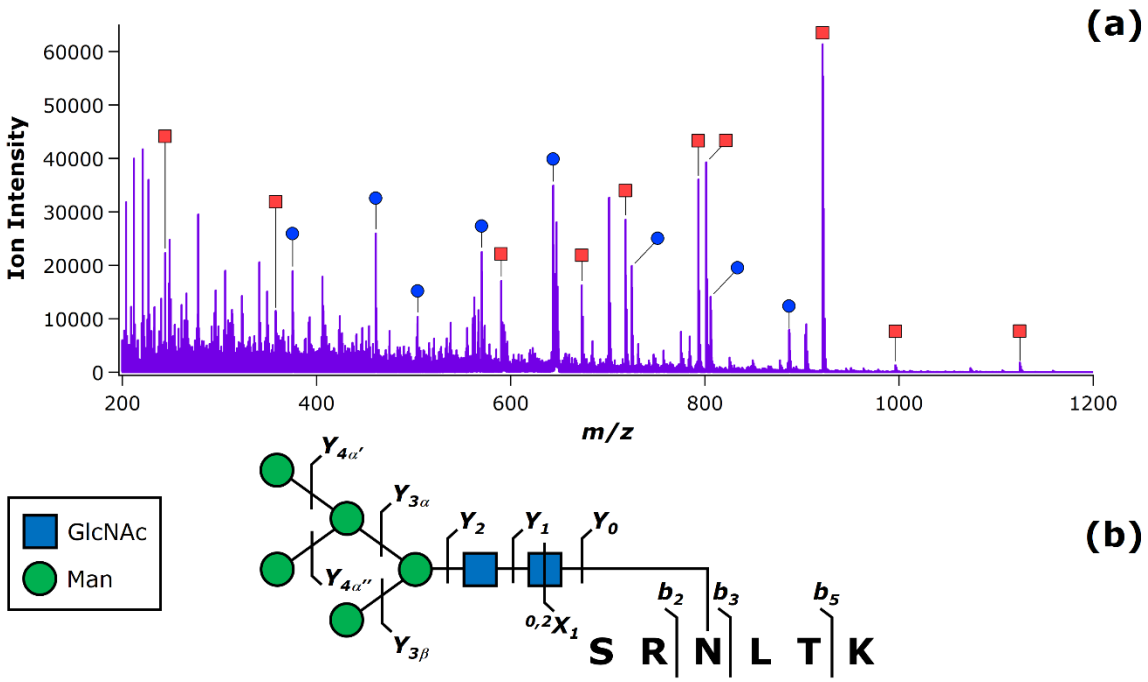

Figure S6. Multi-energy CID of the triply protonated BRB glycopeptide. The CID spectrum **(a)** was acquired via online switching between two collision energies: ΔU = 10.0 V and ΔU = 40.0 V. These correspond to the collision energies applied in **Figure S3a** and **Figure S3c**, respectively. Peak assignments are the same as those shown in **Figure S3a** (labeled here with blue circles) and **Figure S3c** (labeled here with red squares). An abundance of both glycan and peptide fragments were observed, as shown in the accompanying diagram **(b)**.

Table S1. CID collision energies (ΔU) corresponding to 50% precursor ion survival, and the corresponding precursor ion charge states (z) and vibrational degrees of freedom (f). The charge state and degrees of freedom corrected 50% precursor ion survival energies are given in the rightmost column, and have each been multiplied by a factor of 100 to yield more convenient figures. Within the glycopeptide compositions, amino acid residues with basic side chains are shown in bold, while the glycosylated asparagine residue is underlined. The number of charge-carrying protons (n_{H+}) are also indicated relative to the number of basic amino acid side chains (n_B).

	Glycopeptide Composition	*z*	*f*	**Δ*U*** **(V)**	**(*z*Δ*U*/*f*) *100**
$n_{H+}>n_B$	[S**K**PAQGYGYLGVF<u>N</u>NS**K**+$GlcNAc_2Man_3Xyl_1Fuc_1$+3H]$^{3+}$	3	1230	14.9	3.63
	[S**R**<u>N</u>LT**K**+$GlcNAc_2Man_5$+3H]$^{3+}$	3	804	5.5	2.05
$n_{H+}=n_B$	[S**K**PAQGYGYLGVF<u>N</u>NS**K**+$GlcNAc_2Man_3Xyl_1Fuc_1$+2H]$^{2+}$	2	1227	38.8	6.32
	[S**R**<u>N</u>LT**K**+$GlcNAc_2Man_5$+2H]$^{2+}$	2	801	26.2	6.54